Catalysis Today 419 (2023) 114154

Contents lists available at ScienceDirect

Catalysis Today

journal homepage: www.elsevier.com/locate/cattod

Nitrogen-doped carbon nanodots deposited on titania nanoparticles: Unconventional near-infrared active photocatalysts for cancer therapy

Ainhoa Madrid [a,b,c,1], Ana Martín-Pardillos [a,b,e,1], Javier Bonet-Aleta [a,b], Maria Sancho-Albero [d], Gema Martinez [a,b,c], Javier Calzada-Funes [a,b], Pilar Martin-Duque [c,e,f], Jesus Santamaria [a,b,c,e], Jose L. Hueso [a,b,c,e,*]

[a] Instituto de Nanociencia y Materiales de Aragon (INMA), (CSIC-Universidad de Zaragoza), Campus Rio Ebro, Edificio I+D, C/ Poeta Mariano Esquillor, s/n, 50018 Zaragoza, Spain
[b] Department of Chemical and Environmental Engineering, University of Zaragoza, C/María de Luna, 3, 50018 Zaragoza, Spain
[c] Networking Research Center in Biomaterials, Bioengineering and Nanomedicine (CIBER-BBN), Instituto de Salud Carlos III; 28029 Madrid, Spain
[d] Department of Molecular Biochemistry and Pharmacology, Istituto di Ricerche Farmacologiche Mario Negri IRCCS, 20156 Milan, Italy
[e] Instituto de Investigación Sanitaria (IIS) de Aragón, Avenida San Juan Bosco, 13, 50009 Zaragoza, Spain
[f] Departamento de Cirugía, Facultad de Medicina, Universidad de Zaragoza, 50009 Zaragoza, Spain

ARTICLE INFO

Keywords:
Carbon dots
Laser pyrolysis
P25
ROS
PDT
NIR
TME
Nitrogen-doping
Upconversion
Glucose

ABSTRACT

Cancer represents a major public health issue and a primary cause of death for the mankind and the search for alternative cancer treatments that assist or alleviate the drawbacks of current cancer therapies remains imperative. Nanocatalytic medicine represents a new discipline that aims at exploiting the unique response of heterogeneous catalysts exposed to unconventional conditions such as those encountered in the tumor microenvironment (TME). Photo-triggered cancer therapies using light-activable catalytic materiales can stimulate and activate multiple biological processes and represent a very promising field of study. Herein, we evaluate the use of carbon nanodots with different composition (CNDs) retrieved by laser pyrolysis as potential near-infrared (NIR) photosensitizers able to activate P25 semiconductor nanostructured photocatalysts. We describe the enhanced photocatalytic response towards glucose conversion and reactive oxygen species (ROS) generation upon irradiation with NIR-LEDs when CNDs doped with heteroatoms were tested. The most active photocatalysts were evaluated in the presence of cancer cells and revealed a promising photodynamic effect under NIR irradiation. This work represents one of the scarce examples of a conventional inorganic photocatalyst containing TiO_2 that is translated into a biomedical application with a successful outcome.

1. Introduction

Cancer continues to be one of the leading causes of death worldwide. By current estimates, in 2030 close to 22 million new cases will be diagnosed and cancer will cause 13 million deaths worldwide [1]. Among current developing cancer therapies, bionanomedicine and heterogeneous catalysis have merged into the Nanocatalytic Medicine approach [2]. This interdisciplinary field takes advantage of the specificity and enabling ability of heterogeneous catalysts to perform chemical reactions in otherwise passive environments. Furthermore, this unconventional therapeutic approach lies on the consideration of the growing tumor microenvironment (TME) as a specific type of reactor. Only in recent years, inorganic and hybrid nanoplatforms have spurred interest to perform abiotic and enzyme-mimicking catalysis inside living systems [3–10]. So far, the use of nanocatalysts for TME-mediated therapy has shown promising results in the following processes: i) bio-orthogonal anticancer pro-drug activation using noble metal NPs [11–13]; ii) accelerated depletion of key analytes essential in the metabolism and homeostasis of cancer cells (i.e. glucose, glutathione, glutamine) [2,6,9,14,15]; iii) in situ generation of short-lived, toxic species (i.e. Reactive oxygen species-ROS) to induce damage in DNA, lipids, proteins or membranes [4,14]. In addition, selective delivery and

* Corresponding author at: Instituto de Nanociencia y Materiales de Aragon (INMA), Campus Rio Ebro, Edificio I+D, C/ Poeta Mariano Esquillor, s/n, 50018 Zaragoza, Spain.
E-mail address: jlhueso@unizar.es (J.L. Hueso).
[1] These authors contributed equally

https://doi.org/10.1016/j.cattod.2023.114154
Received 30 January 2023; Received in revised form 30 March 2023; Accepted 6 April 2023
Available online 7 April 2023

remote activation of the catalytic function after it has reached the TME also pose as highly challenging objectives [16,17].

Photocatalysts are among the nanomaterials with multifunctional redox activity that can be remotely activated in the presence of light to induce the generation of ROS. Semiconductors based on SnO_x and TiO_2 exhibit good activity toward biomass and carbohydrate photo-induced conversion [18,19]. The major shortcoming associated to their limited response beyond the UV- region has been overcome by the addition of organic photosensitizers [20–24], metallic co-catalysts [7,25–29] or the induced generation of defects and vacancies in the semiconductor oxides (e.g. blue and black titania) [30–32]. The redox ability of titania to produce ROS is well established and a number of increasing studies has additionally exploited the strong affinity between titania and glucose [26,33–37] to carry out the photoreforming of the carbohydrate as sacrificial agent to produce hydrogen [38]. Still, the number of titania-based catalysts able to perform under the TME constraint conditions upon remote triggering by external stimuli is scarce [18,39–42]. This work aims at exploring the potential role of P25 nanoparticles (NPs) to simultaneously form ROS and deplete glucose in the unconventional TME. To do so, we have taken advantage of the versatility of carbon nanodots (CNDs) as organic sensitizers able to activate P25 NPs and expand their photocatalytic response towards the visible-NIR range

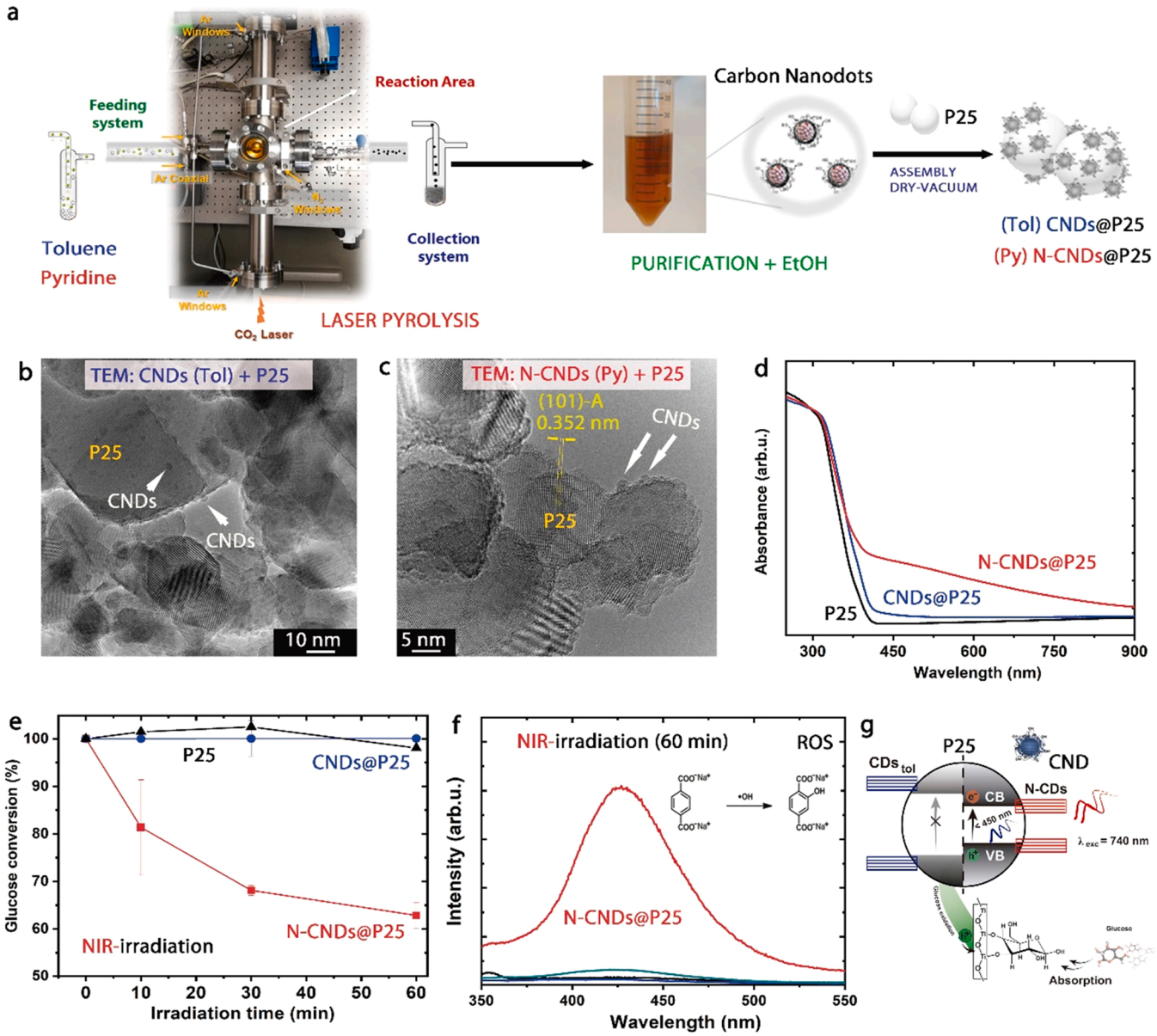

Fig. 1. Laser-assisted synthesis of CNDs, assembly and photocatalytic response under LED-NIR illumination: a) Scheme of the laser pyrolysis of toluene and pyridine using an infrared CO_2 continuous laser source; the particles are collected in TREG, purified after centrifugation and assembled onto P25 NPs; b) High-Resolution TEM image of the CNDs@P25 composites obtained from the toluene feed; white arrows are indicative of representative examples of CNDs attached to the P25 NPs; c) HR-TEM of the N-CNDs@P25 hybrids retrieved from the pyridine feed; lattice fringes at 0.352 nm corresponding to (101) anatase planes are also indicated; d) UV-Vis absorption spectra of the P25 NPs before (black) and after assembly with the undoped (blue) and N-doped CNDs (red), respectively; e) NIR-driven photocatalytic conversion glucose in the presence of P25 NPs before and after assembly with the undoped and N-doped CNDs; f) Evaluation of the in situ generation of hydroxyl radicals upon photoirradiation (time = 60 min) with a high radiance NIR-LED (λ_{exc}= 740 nm) in the presence of P25 NPs before and after assembly with undoped and doped CNDs using disodium terephthalate (NaTA) as fluorescent probe selective to $^{\bullet}OH$ radicals; g) Schematic display of the role of CNDs as photosensitizers able to delay the electron-hole recombination rates of P25 and provide positive charges for the specific conversion of glucose molecules that tend to assembly well onto the surface of the titania support.

[43–46].

In the past two decades, the study of CNDs has flourished based on their excellent optical and photocatalytic activity, providing a successful range of applications both in the environmental and biomedical fields. Interestingly, the optical behavior of CNDs can be tuned up by the presence of doping heteroatoms such as N, P or S [43] and most recently Fe [47]. Nitrogen-doping of CNDs represents the most exploited alternative to modify CNDs and previous studies have established that depending on the level of substitution and the type of bond, the energy levels of the carbogenic dots provide different optical response [42,43,48]. The upconversion response of these N-CNDs has boosted their application toward the environmental remediation of organic pollutants taking advantage of the full-solar spectrum [37,42,46,49,50]. Alternatively, N-CNDs have been successfully exploited as theranostic agents able to simultaneously act as NIR-bioimaging markers and photodynamic agents able to induce the generation of ROS preferentially in cancer cells [45,48,51]. In this work, we have taken advantage of the exquisite control of the laser pyrolysis of liquid precursors to obtain undoped and N-doped CNDs [42]. This synthesis strategy enables a controlled doping of the generated carbon nanostructures with light elements (i.e. N, S, F) to tune their photoluminescence (PL) properties. We have assembled these CNDs onto P25 NPs and tested them against the photocatalytic conversion of glucose, the generation of hydroxyl radicals and for *in cellulo* photocatalytic tests to treat glioblastoma cells (U251-MG) using Near-Infrared (NIR) light remote stimuli.

2. Results and discussion

2.1. Synthesis of the photocatalysts and NIR-driven tests for glucose conversion and ROS generation under cell-free conditions

A schematic display of the synthesis of the CNDs and their assembly onto P25 NPs is summarized in Fig. 1a. The synthesis of undoped and N-doped CNDs was carried out by laser pyrolysis of toluene and pyridine using precursor concentrations, gas flow rates and working pressures similar to those reported by Mas et al. [42] and summarized in Table S1. A higher laser power of 275 W was applied to obtain the CNDs reported in this work (Table S1). Toluene or pyridine were fed into the reaction chamber from a sealed vessel equipped with regulatory opening-close valves. Sulfur hexafluoride (SF_6) was fed to sensitize the infrared laser (CO_2, $\lambda = 10.6$ μm) and Argon (Ar) was used as carrier gas passing through the organic precursor reservoir. The laser was placed to interact with the reactant streams in a 90 ° configuration, thereby providing well-defined residence times, with fast activation and post reaction quenching [42,52–54]. The as-prepared NPs were directly collected in a liquid trap containing triethylenglycol (TREG) that helped to improve their stability when resuspended in aqueous media. Transmission electron microscopy (TEM) revealed similar mean diameters of ca. 1.9 nm for both CNDs retrieved from toluene and pyridine pyrolysis, respectively (Fig. S1a). High resolution TEM analysis and XRD further confirmed the crystalline nature of the CNDs exhibiting characteristic lattice fringes of graphite (Fig. S1b-S1d). XPS revealed a higher content of N in the surface of the carbon nanodots retrieved from pyridine (hereafter labelled N-CNDs) (see Fig. S2). In addition, a marginal presence of S and F was also detected and attributed to partial decomposition of the sensitizer used during the laser pyrolysis (SF_6). The presence of a higher fraction of C-N/C-O bonds in the C1s region of the N-CNDs was also indicative of higher disorder degree due to the higher fraction of sp3 bonds (Fig. S2b-S2e) induced by the major presence of defects and/or intercalation of N atoms. Raman spectroscopy also corroborated the increased presence of defects, stacking faults, lack of symmetry and impurities in the N-CNDs retrieved from pyridine (Fig. S3). The fitted Raman bands typically associated to carbon defects were more prominent in comparison with the CNDs from toluene (see Fig. S3).

The assembly of the CNDs onto P25 NPs was carried out following a protocol described elsewhere for anatase [42,44]. It consisted on heating and drying under vacuum a suspension of the resulting CNDs and the commercial P25 NPs (see Experimental section for further details). HR-TEM images shown in Figs. 1b-1c accounted for the successful attachment and homogeneous distribution of the CNDs (some of them highlighted by white arrows for the sake of clarity) onto the P25 NPs. Remarkably, the addition of the CNDs expanded the UV-Vis-NIR absorption spectrum of commercial P25 NPs towards the visible-NIR range (Fig. 1d). This effect became especially evident with the N-doped CNDs. Nitrogen doping is able to introduce additional energy levels that couple with the TiO_2 energy levels, thereby reducing their energy band gap and allowing the absorption of additional photons with lower energy. It may also favor anti-Stokes luminescence shifts that do not require large fractions of coherent photons (i.e. upconversion vs two-photon absorption) [43–46].

The naked P25 NPs and the corresponding composites containing the CNDs were tested as potential photocatalysts for glucose conversion under LED-NIR irradiation at 740 nm. The initial dispersion of the CNDs in TREG helped to improve their stability in aqueous suspensions for the photocatalytic tests. Reducing the glucose levels to induce starvation in cancer cells with a highly glucose-dependent metabolism represents an interesting therapeutic strategy and the use of light stimulation in the NIR transparent biological window (i.e. higher penetration depth) is also extremely convenient for remotely triggered photodynamic processes in spatially localized targets [18,39,55]. Fig. 1e shows the evolution of the glucose levels at different irradiation intervals. The commercial P25 NPs and the corresponding composite decorated with the CNDs retrieved from toluene pyrolysis (i.e. undoped) exhibited a negligible photo-activity and no glucose was converted. In contrast, the N-CND@P25 catalyst was able to yield up to 45% glucose conversion after 60 min of NIR-illumination (Fig. 1e and Fig. S4). Analogous glucose photo-conversion levels have been recently reported by Da Vià et al.[56] using P25 NPs under UV and visible light irradiation but not reported the use of NIR illumination sources. Other recent articles have also reported the photo-reforming of glucose and biomass derivatives as a sacrificial electron donor to favour a green alternative to generate H_2 [19,38,57–59]. Most of these studies attribute their positive results to the great chemical affinity of the glucose molecule to accommodate onto the surface of TiO_2 forming either a mono or a bidentate complex able to transfer electrons and expand the response of P25 towards the visible range [34,35,37,56,59] (Fig. 1 g). In our case, the specific photocatalytic response under NIR illumination must be attributed to the role of N-doped CNDs as photosensitizers and light harvesters [42,47]. This role of CNDs has been previously reported in other TiO_2-based photocatalysts containing N-doped CNDs [34,42–44,59,60], in TiO_2 networks doped with heteroatoms [30,38,61], in O_2-deficient or hydrogenated TiO_2 NPs [31,62] or in different semiconductors (ZnO, SnO_2 or TiO_2) containing porphyrazines or upconverting lanthanides [20,24,63].

The glucose conversion must be driven by the generation of reactive electron-hole pairs leading to the formation of ROS. ROS generation has become another important strategy to tackle cancer by PDT and the capacity to locally induce ROS via an external stimuli [5] (i.e. light, ultrasounds, microwaves, magnetic field, X-rays, γ-rays) may represent an enormous advantage with nanostructured catalysts that take advantage of the enhanced permeation and retention (EPR) effect in the TME [18]. Therefore, we evaluated the specific capacity of each of the photocatalysts to generate hydroxyl radicals ($^{\bullet}OH$) under NIR illumination using disodium terephthalate (NaTA) as fluorescent probe selective to $^{\bullet}OH$ radicals [44,45,48]. Fig. 1f shows that only the N-CND@P25 NPs exhibited a significant photo-activity to form the fluorescent hydroxylated compound after 60 min of NIR irradiation. These results further addressed that only the CNDs retrieved from the laser-assisted pyrolysis of pyridine were responsive to the NIR wavelengths, as observed in the glucose conversion experiments. We can assume that N atoms provide additional electronic levels that accommodate below the conduction band of P25 reducing its intrinsic energy bandgap. In addition, it has been also reported that N-doped CNDs may hold upconversion

capabilities to harvest longer wavelength photons and convert them into more energetic emissive photons [43–46,48,60,64,65] (Fig. 1 g). In this regard, the photoluminescence (PL) spectra of both the undoped and N-doped CNDs corroborated the upconversion response of the latter when excited at 740 nm (Fig. S5). As a result, this latter photocatalyst combining the synergistic action of N-doped CNDs and P25 NPs was selected to perform photocatalysis with cancer cells.

2.2. Internalization and photocatalytic tests in cancer cells under NIR-irradiation

The tolerability of cancer cells (U251-MG) to the exposure of increasing amounts of N-CND@P25 NPs was determined by incubating the photocatalyst with the respective cells during 6, 24 and 48 h, respectively. Fig. 2a shows that no signs of cytotoxicity were found at any of the catalyst concentrations evaluated for all the incubation periods. Optical images revealed an elevated internalization of NPs at concentrations of 0.1 mg mL^{-1} and this value was selected in the subsequent experiments (Fig. 2b). The internalization of N-CND@P25 NPs into U251-MG cells was further assessed by confocal microscopy. Fig. 2c includes representative images from U251-MG cells, after incubation with the photocatalyst for 4, 6, 8, 10, 24 and 48 h. A significant accumulation of N-CND@P25 NPs inside the U251-MG cells was preferentially observed in the 8–10 h incubation window (Fig. 2c). The internalization route was evaluated by marking lysosomes and CD63 positive endosomes and investigating their co-localization with N-CND@P25 NPs under confocal microscopy. The results (see the Z-stack sections of the images in Fig. 2c) confirmed the localization of the N-CND@P25 NPs via an endosomal pathway, with preference to the lysosomal route.

U251-MG cells were treated with 0.1 mg N-CND@P25 NPs·mL^{-1} during 24 h following by 10 or 30 min irradiation with the NIR-LED light. The identification of ROS species was monitored by confocal microscopy using a CellROX kit (see Figs. 3a-3b and Experimental section in SI for further details). The production of intracellular ROS and the potential effect of NIR irradiation itself was negligible in the absence of N-CND@P25 NPs, regardless of the selected irradiation time (Figs. 3a-3b) [66]. In contrast, cells treated with N-CND@P25 NPs showed a

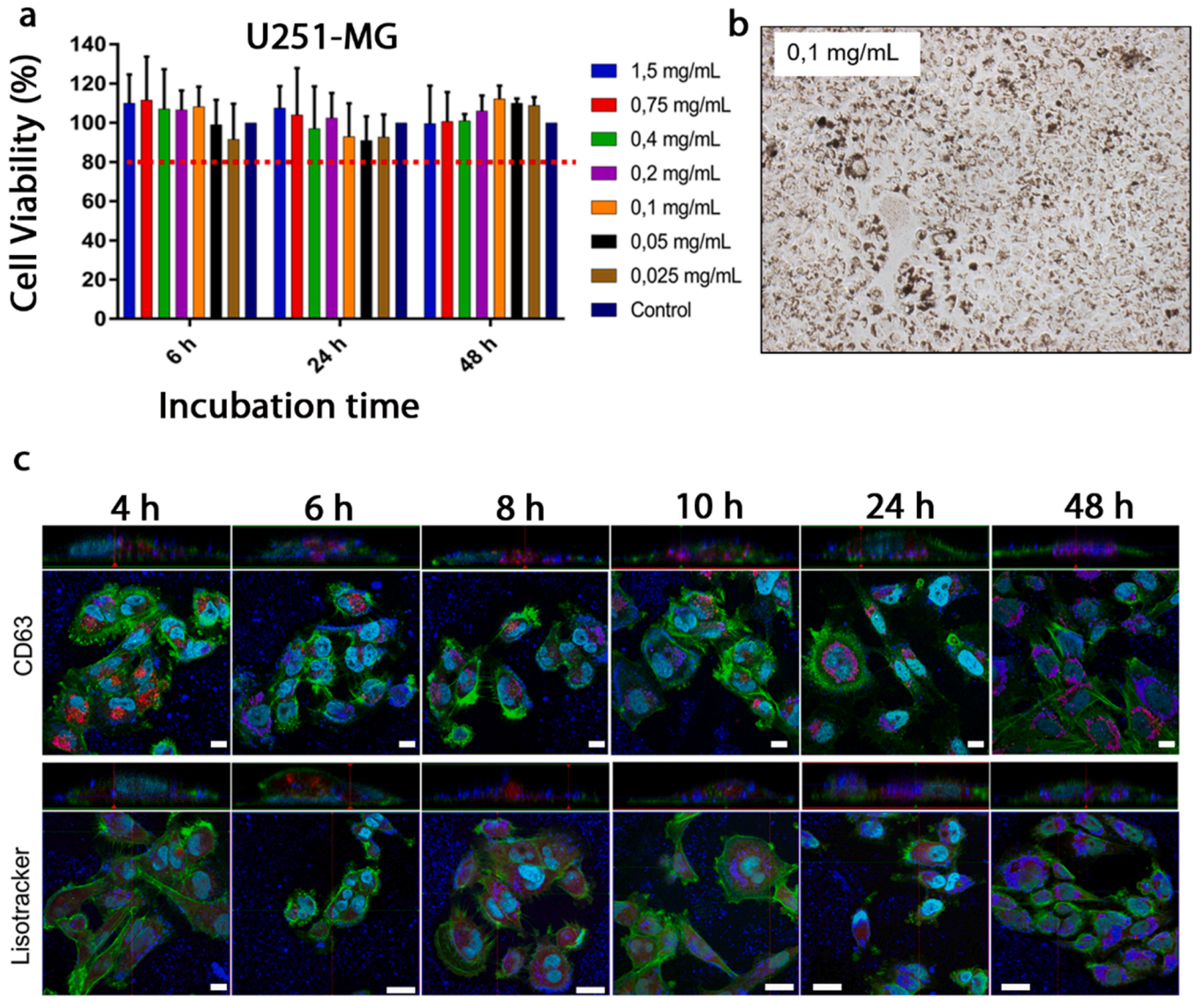

Fig. 2. Internalization, cell viability and trafficking of N-CND@P25 nanohybrids in the presence of U251-MG cells: a) Tolerability study of N-CND@P25 NPs incubated with U251-MG cells after 6 h, 24 h and 48 h (n = 4); b) Optical microscopy image corresponding to U251-MG cells after 48 h incubation with a concentration of 0.1 mg·mL^{-1} of N-CND@P25 NPs; c) Evaluation of the internalization strategy of the N-CND@P25 NPs by in vitro confocal trafficking study of the endosomal and lisosomal pathways. Cross and top view images of U251-MG cells incubated with 0.1 mg·mL^{-1} of N-CND@P25 NPs during 4, 6, 10, 24 and 48 h; Actin appears in green, nuclei in cyan, N-CND@P25 in blue and CD63 positive vesicles in red. Scale = 20 μm.

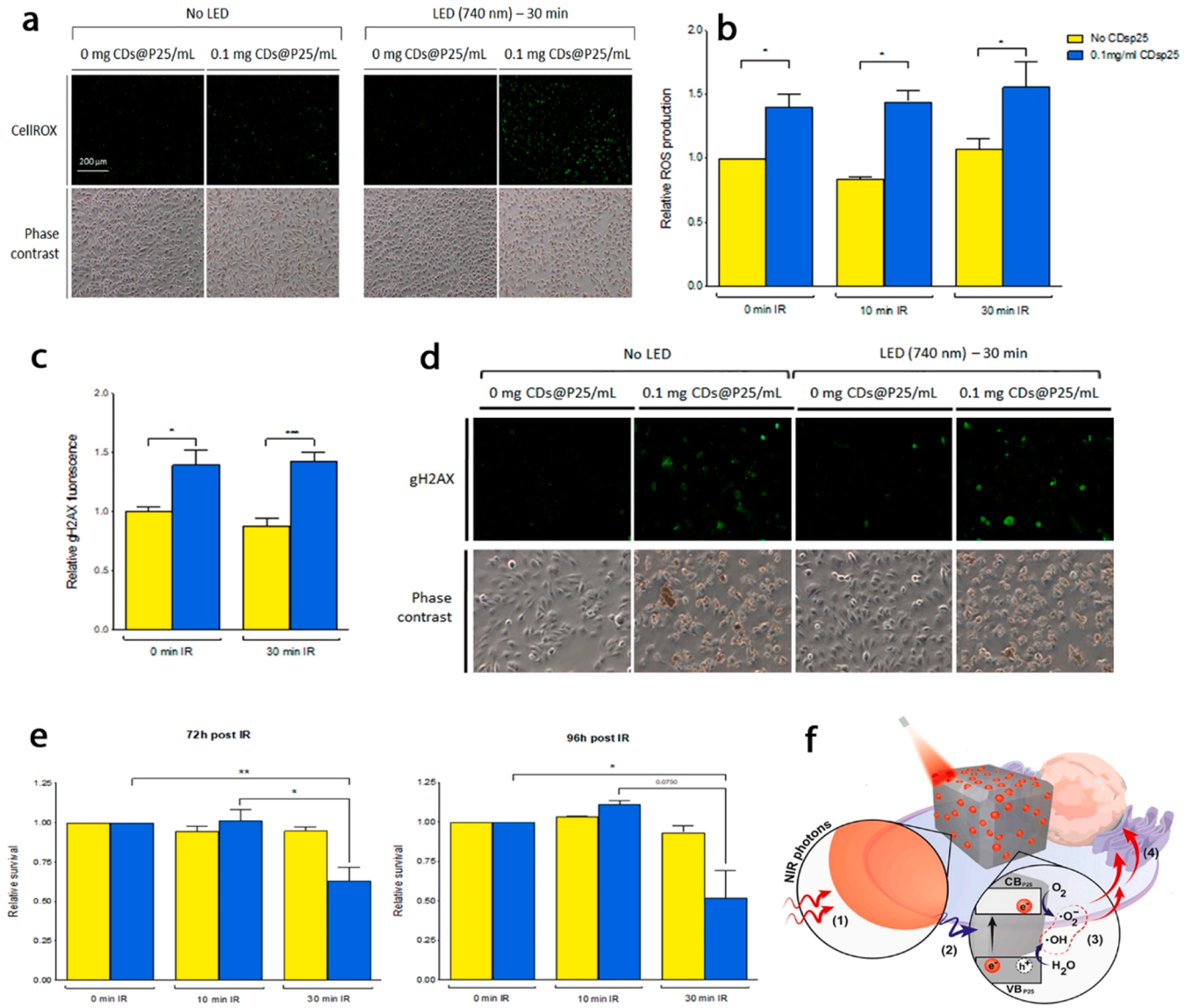

Fig. 3. Reactivity of the N-CNDs@P25 NPs with U251-MG cancer cells after irradiation with NIR light: a) Confocal images illustrating the generation of intracellular ROS after NIR-LED (740 nm) irradiation in the absence and in the presence of N-CNDs@P25 NPs in U251MG cells; Negative control treatment correspond to non-treated cells (no photocatalyst added) and negative control irradiation (non-irradiated photocatalyst). Irradiation time: 30 min; Phase contrast as displayed in grey tones and ROS species are detected with a CellROX staining (green); b) Quantification of fluorescence generated by CellROX dye both in the absence and presence of photocatalyst without irradiation and after 10 or 30 min of NIR illumination, respectively. Scale bar: 200 µm; c) Generation of DNA damage: Phase contrast and fluorescence images corresponding to DNA damage marker (gH2AX). Images of negative irradiation controls (No LED), as well as non-treated cells (no photocatalyst), are shown against cells loaded with N-CNDs@P25 NPs (previously treated with 0.1 mg·mL^{-1}). Irradiation times: 0 and 30 min. Scale bar 200 µm; d) Quantification of DNA damage activation by gH2AX fluorescence; e) Viability of U251-MG cells after NIR-irradiation in the absence and presence of N-CNDs@P25 NPs. Comparison between non-irradiated cells and irradiated cells, non-treated cells (No photocatalyst) and loaded with N-CNDs@P25 NPs (pre-treated with 0.1 mg·mL^{-1}). After LED irradiation cells were kept in culture during 72 h and 96 h, respectively; cell survival were determined by measurement of the metabolic activity. Obtained values were relativized to non-irradiated cells; f) Schematic illustration of the proposed intracellular reaction mechanism of the N-CNDs@P25 NPs, including photo-excitation under NIR-irradiation (1) and (2) to generate reactive electron-hole pairs that further react leading to ROS production (3) to induce irreversible DNA damage (4) reducing the viability of the cancer cells.

significant increase of ROS production compared to non-treated cells, even without irradiation (Figs. 3a-3b). N-CNDs and P25 NPs induced intracellular ROS generation in a dose dependent manner, even in the absence of light activation, as it has been previously described [41,55,65,67–72]. Still, the intracellular production of ROS increased upon activation of the N-CND@P25 NPs under 740 nm LED light in a time-dependent manner (Figs. 3a-3b).

Since the generation of ROS is directly related to the induction of DNA damage, DNA damage response activation and reduction of cell viability was also evaluated [73,74]. It has been previously reported that eukaryotic cells phosphorylate the subtype of histone H2A, called H2AX, in the position of Ser139 occurs in response to DNA damage, generating the phosphorylated form called γH2AX [75]. Having demonstrated the generation of ROS after incubation with N-CND@P25 NPs, we proceeded to determine the generation of DNA damage by detecting γH2AX. Since the γH2AX response is maximal 30 min after exposure of damage and declines over a period of hours as the cells repair the damage [76–78], we examined the γH2AX foci 30 min after irradiation. As we show in Figs. 3c-3d and Fig. S6, a significant increase in γH2AX foci was observed in cells treated with N-CND@P25 NPs, which showed that the generation of ROS by N-CND@P25 NPs induced DNA damage. However the phosphorylation of the histone, H2AX, has not been related

with RNA damage. In fact, RNA polymerases and RNA itself have been implicated at various stages of the DNA damage repair, including damage sensing, recruitment of DNA repair factors and tethering of broken DNA ends. Therefore, DNA damage do not affect to the RNA, and the RNA may even serve as a template for DNA repair under certain conditions [79]. No significant differences were observed between irradiated and non-irradiated cells treated with N-CND@P25 NPs. These results are in agreement with the trend observed with the intracellular ROS generation levels (Figs. 3a-3b). We could confirm that the ROS generated by the N-CND@P25 NPs led to DNA damage but it has been also extensively reported that the consequences of DNA damage depend on the severity of the damage. Mild DNA damage can be repaired with or without cell-cycle arrest, although more severe and irreparable DNA damage leads to cell cycle arrest [80]. Therefore, we proceeded to monitor and analyze the severity of the DNA damage induced by the N-CND@P25 NPs and the NIR irradiation and their consequences on cell survival.

With this aim, cells were irradiated during 10 and 30 min and maintained in culture for 72 and 96 h, determining their viability at these time intervals. LED irradiation did not induce decrease of cell viability in non-treated cells due to the absence of ROS generation (Fig. 3e). A 10 min NIR irradiation did not induce a significant decrease of cell viability in U251-MG cells loaded with N-CND@P25 NPs (Fig. 3e). In contrast, increasing up to 30 min the NIR irradiation led to a significant decrease of the viability 72 and 96 h after the initial activation by the NIR-LED (up to 40% and 50% respectively) (see Fig. 3e). We can conclude that even though the only presence of N-CND@P25 NPs without irradiation was enough to induce ROS, the DNA damage was mild and reversible and it could be repaired by the DNA damage response pathways (Fig. 3e). In contrast, longer NIR irradiations induced a more severe DNA damage, able to decrease the cellular viability of U251-MG cells (Fig. 3e). These results show how N-CND@P25 NPs under light activation can be useful to treat cancer, decreasing the survival of tumor cells, thereby translating the activity of a conventional photocatalyst typically devoted to environmental catalysis into a less conventional application scenario against the TME. We ran an additional set of analogous irradiation experiments with uncoated P25 NPs, leading to a much less significant cell damage after 72 and 96 h (Fig. S7). Therefore, although the influence of P25 NPs in the reduction of cell viability at 96 h cannot be ruled out as previously described Long et al. [81], we can conclude that N-CNDs provide a synergistic and phototherapeutic activity that can be tentatively attributed to the combination of ROS generation and irreversible DNA damage (Fig. 1 f). In addition, the affinity and photo-reactivity between N-CND@P25 NPs and glucose can be another potential reason of interference in the regulation of glucose uptake. Fig. S8 shows the glucose percentages determined in the U251-MG cell media after 24 h of incubation and how only the NIR stimulation of the photocatalyst affected the glucose levels.

3. Conclusions

Laser pyrolysis of different solvents such as toluene and pyridine that hold a similar chemical structure mainly differentiated by the presence of N induces the generation of CNDs with different optical behavior, especially in the NIR window. Nitrogen-doping of the CNDs retrieved from the laser-driven pyrolysis of pyridine is able to harvest light in the NIR region and favors the expanded photocatalytic response of P25 NPs under NIR excitation towards the efficient conversion of glucose and the generation of ROS. Remarkably, this photocatalyst can be successfully internalized in glioblastoma cells and induce their irreversible death after illumination with NIR light. This work represents an alternative use of conventional photocatalysts into a less conventional reaction scenario involving the tumor microenvironment. The use of alternative photodynamic agents based on regular photocatalysts paves the way to novel and promising routes where the use of composites with a well-controlled design can be strongly beneficial to regulate and alter the homeostasis and metabolism of cancer cells upon on-demand stimulation. CNDs represents one of the most promising and versatile alternative as co-catalyst with a photosensitizing role and broad-range of light response. In addition, P25 appear as attractive photocatalytic platforms to regulate glucose upon remote light triggering, thereby opening new potential avenues in the area of starvation therapy.

CRediT authorship contribution statement

Ainhoa Madrid: Methodology, Validation, Formal analysis, Investigation; **Ana Marín-Pardillos:** Methodology, Validation, Formal analysis, Investigation, Data curation, Writing – original draft, Visualization, Writing – review and editing; **Javier Bonet-Aleta:** Methodology, Validation, Formal analysis, Investigation, Writing – review and editing; **Maria Sancho-Albero:** Methodology, Validation, Formal analysis, Investigation, Writing – review and editing; **Gema Martinez**: Conceptualization, Methodology, Investigation, Supervision; **Javier Calzada-Funes:** Methodology, Formal analysis, Investigation; **Pilar Martin-Duque:** Methodology, Visualization, Supervision, Funding, Writing – review and editing; **Jesus Santamaria:** Conceptualization, Methodology, Supervision, Funding acquisition, Writing – review and editing; **Jose L. Hueso:** Conceptualization, Methodology, Validation, Formal analysis, Investigation, Data curation, Writing – original draft, Writing – review and editing, Visualization, Supervision, Funding acquisition.

Declaration of Competing Interest

The authors declare that they have no known competing financial interests or personal relationships that could have appeared to influence the work reported in this paper.

Data availability

Data will be made available on request.

Acknowledgments

Financial support from the European Research Council (ERC-Advanced Grant CADENCE number 742684), the FP7 People Program (NANOLIGHT-294094), the Spanish Research Agency (LAERTES-PID2020–114926RB-I00) and Instituto de Salud Carlos III (ISCIII) (PI19/01007 and DTS21/00130) are acknowledged. The TEM measurements were conducted at the Laboratorio de Microscopias Avanzadas, ICTS ELECMI, Spain. The synthesis of materials has been performed by the Platform of Production of Biomaterials and Nanoparticles of the NANBIOSIS ICTS, more specifically by the Nanoparticle Synthesis Unit of the CIBER in BioEngineering, Biomaterials & Nanomedicine (CIBER-BBN). The authors also thank the Scientific and Technical Services at CIBA (IACS), especially tissue culture, and microscopy for the technical support. J.B-A. acknowledges the Spanish Government for an FPU predoctoral contract.

Appendix A. Supporting information

Supplementary data associated with this article can be found in the online version at doi:10.1016/j.cattod.2023.114154.

References

[1] WHOWorld Health Organization: Global Health Estimates 2020: Deaths by Cause, Age, Sex, by Country and by Region, 2000–2019, World Health Organization: Global Health Estimates 2020: Deaths by Cause, Age, Sex, by Country and by Region, 2000–2019, (2020).
[2] B.W. Yang, Y. Chen, J.L. Shi, Nanocatalytic medicine, Adv. Mater. 31 (2019).
[3] C. Adamson, M. Kanai, Integrating abiotic chemical catalysis and enzymatic catalysis in living cells, Org. Biomol. Chem. 19 (2021) 37–45.
[4] Z.M. Tang, P.R. Zhao, H. Wang, Y.Y. Liu, W.B. Bu, Biomedicine meets Fenton chemistry, Chem. Rev. 121 (2021) 1981–2019.

[5] J.I. Garcia-Peiro, J. Bonet-Aleta, J. Santamaria, J.L. Hueso, Platinum nanoplatforms: classic catalysts claiming a prominent role in cancer therapy, Chem. Soc. Rev. 51 (2022) 7662–7681.
[6] J. Bonet-Aleta, M. Encinas-Gimenez, E. Urriolabeitia, P. Martin-Duque, J.L. Hueso, J. Santamaria, Unveiling the interplay between homogeneous and heterogeneous catalytic mechanisms in copper-iron nanoparticles working under chemically relevant tumour conditions, Chem. Sci. 13 (2022) 8307–8320.
[7] J.C. Yang, H.L. Yao, Y.D. Guo, B.W. Yang, J.L. Shi, Enhancing tumor catalytic therapy by co-catalysis, Angew. Chem. -Int. Ed. 61 (2022).
[8] C.Y. Wu, D.L. Xu, M. Ge, J.J. Luo, L.S. Chen, Z.X. Chen, Y.L. You, Y.X. Zhu, H. Lin, J.L. Shi, Blocking glutathione regeneration: Inorganic NADPH oxidase nanozyme catalyst potentiates tumoral ferroptosis, Nano Today 46 (2022).
[9] J.J. Shi, P.W. Kantoff, R. Wooster, O.C. Farokhzad, Cancer nanomedicine: progress, challenges and opportunities, Nat. Rev. Cancer 17 (2017) 20–37.
[10] L.Y. Wang, M.F. Huo, Y. Chen, J.L. Shi, Tumor microenvironment-enabled nanotherapy, Adv. Healthc. Mater. 7 (2018).
[11] B. Rubio-Ruiz, A.M. Perez-Lopez, L. Uson, M.C. Ortega-Liebana, T. Valero, M. Arruebo, J.L. Hueso, V. Sebastian, J. Santamaria, A. Unciti-Broceta, In Cellulo bioorthogonal catalysis by encapsulated aupd nanoalloys: overcoming intracellular deactivation, Nano Lett. (2023).
[12] S.Y. Chow, A. Unciti-Broceta, Targeted molecular construct for bioorthogonal theranostics of PD-L1-expressing cancer cells, JACS Au 2 (2022) 1747–1756.
[13] M. Sancho-Albero, B. Rubio-Ruiz, A.M. Perez-Lopez, V. Sebastian, P. Martin-Duque, M. Arruebo, J. Santamaria, A. Unciti-Broceta, Cancer-derived exosomes loaded with ultrathin palladium nanosheets for targeted bioorthogonal catalysis, Nat. Catal. 2 (2019) 864–872.
[14] B.W. Yang, Y. Chen, J.L. Shi, Reactive oxygen species (ROS)-based nanomedicine, Chem. Rev. 119 (2019) 4881–4985.
[15] H. Lin, Y. Chen, J.L. Shi, Nanoparticle-triggered in situ catalytic chemical reactions for tumour-specific therapy, Chem. Soc. Rev. 47 (2018) 1938–1958.
[16] M. Sancho-Albero, N. Navascues, G. Mendoza, V. Sebastian, M. Arruebo, P. Martin-Duque, J. Santamaria, Exosome origin determines cell targeting and the transfer of therapeutic nanoparticles towards target cells, J. Nanobiotechnol. 17 (2019).
[17] M. Sancho-Albero, Md.M. Encabo-Berzosa, M. Beltran-Visiedo, L. Fernandez-Messina, V. Sebastian, F. Sanchez-Madrid, M. Arruebo, J. Santamaria, P. Martin-Duque, Efficient encapsulation of theranostic nanoparticles in cell-derived exosomes: leveraging the exosomal biogenesis pathway to obtain hollow gold nanoparticle-hybrids, Nanoscale 11 (2019) 18825–18836.
[18] J. Shi, J. Li, Y. Wang, C.Y. Zhang, TiO2-based nanosystem for cancer therapy and antimicrobial treatment: a review, Chem. Eng. J. 431 (2022).
[19] H. Zhao, X.T. Yu, C.F. Li, W.B. Yu, A.G. Wang, Z.Y. Hu, S. Larter, Y. Li, M.G. Kibria, J.G. Hu, Carbon quantum dots modified TiO2 composites for hydrogen production and selective glucose photoreforming, J. Energy Chem. 64 (2022) 201–208.
[20] M. Cheng, Q. Zhang, C. Yang, B. Zhang, K. Deng, Photocatalytic oxidation of glucose in water to value-added chemicals by zinc oxide-supported cobalt thioporphyrazine, Catal. Sci. Technol. 9 (2019) 6909–6919.
[21] C.C. Yang, C.X. Wang, C.Y. Kuan, C.Y. Chi, C.Y. Chen, Y.Y. Lin, G.S. Chen, C. H. Hou, F.H. Lin, Using C-doped TiO2 nanoparticles as a novel sonosensitizer for cancer treatment, Antioxidants 9 (2020).
[22] H. Hao, J.-L. Shi, H. Xu, X. Li, X. Lang, N-hydroxyphthalimide-TiO2 complex visible light photocatalysis, Appl. Catal. B-Environ. 246 (2019) 149–155.
[23] X. Li, H. Xu, J.-L. Shi, H. Hao, H. Yuan, X. Lang, Salicylic acid complexed with TiO2 for visible light-driven selective oxidation of amines into imines with air, Appl. Catal. B-Environ. 244 (2019) 758–766.
[24] Q. Zhang, Y. Ge, C. Yang, B. Zhang, K. Deng, Enhanced photocatalytic performance for oxidation of glucose to value-added organic acids in water using iron thioporphyrazine modified SnO2, Green. Chem. 21 (2019) 5019–5029.
[25] H. Okatsu, N. Kinoshita, T. Akita, T. Ishida, M. Haruta, Deposition of gold nanoparticles on carbons for aerobic glucose oxidation, Appl. Catal. a-Gen. 369 (2009) 8–14.
[26] L. Da Via, C. Recchi, T.E. Davies, N. Greeves, J.A. Lopez-Sanchez, Visible-light-controlled oxidation of glucose using titania-supported silver photocatalysts, Chemcatchem 8 (2016) 3475–3483.
[27] X. Ye, X.Y. Shi, H. Zhong, T.F. Wang, J. Duo, B.B. Jin, F.M. Jin, Photothermal strategy for the highly efficient conversion of glucose into lactic acid at low temperatures over a hybrid multifunctional multi-walled carbon nanotube/layered double hydroxide catalyst, Green. Chem. 24 (2022) 813–822.
[28] X. Jin, M. Zhao, J. Shen, W.J. Yan, L.M. He, P.S. Thapa, S.Q. Ren, B. Subramaniam, R.V. Chaudhari, Exceptional performance of bimetallic Pt1Cu3/TiO2 nanocatalysts for oxidation of gluconic acid and glucose with O-2 to glucaric acid, J. Catal. 330 (2015) 323–329.
[29] M.C. Ortega-Liebana, J.L. Hueso, R. Arenal, J. Santamaria, Titania-coated gold nanorods with expanded photocatalytic response. Enzyme-like glucose oxidation under near-infrared illumination, Nanoscale 9 (2017) 1787–1792.
[30] R. Asahi, T. Morikawa, T. Ohwaki, K. Aoki, Y. Taga, Visible-light photocatalysis in nitrogen-doped titanium oxides, Science 293 (2001) 269–271.
[31] X.B. Chen, L. Liu, P.Y. Yu, S.S. Mao, Increasing solar absorption for photocatalysis with black hydrogenated titanium dioxide nanocrystals, Science 331 (2011) 746–750.
[32] Y.H. Hu, A highly efficient photocatalysthydrogenated black TiO2 for the photocatalytic splitting of water, Angew. Chem. -Int. Ed. 51 (2012) 12410–12412.
[33] J. Park, G.H. Moon, K.O. Shin, J. Kim, Oxalate-TiO2 complex-mediated oxidation of pharmaceutical pollutants through ligand-to-metal charge transfer under visible light, Chem. Eng. J. 343 (2018) 689–698.
[34] I. Abdouli, M. Eternot, F. Dappozze, C. Guillard, N. Essayem, Comparison of hydrothermal and photocatalytic conversion of glucose with commercial TiO2: Superficial properties-activities relationships, Catal. Today 367 (2021) 268–277.
[35] G. Kim, S.-H. Lee, W. Choi, Glucose-TiO2 charge transfer complex-mediated photocatalysis under visible light, Appl. Catal. B-Environ. 162 (2015) 463–469.
[36] G. Kim, W. Choi, Charge-transfer surface complex of EDTA-TiO2 and its effect on photocatalysis under visible light, Appl. Catal. B-Environ. 100 (2010) 77–83.
[37] G. Zhang, G. Kim, W. Choi, Visible light driven photocatalysis mediated via ligand-to-metal charge transfer (LMCT): an alternative approach to solar activation of titania, Energy Environ. Sci. 7 (2014) 954–966.
[38] R. Shi, Z. Li, H.J. Yu, L. Shang, C. Zhou, G.I.N. Waterhouse, L.Z. Wu, T.R. Zhang, Effect of nitrogen doping level on the performance of n-doped carbon quantum dot/TiO2 composites for photocatalytic hydrogen evolution, Chemsuschem 10 (2017) 4650–4656.
[39] X.W. Wang, X.Y. Zhong, L. Cheng, Titanium-based nanomaterials for cancer theranostics, Coord. Chem. Rev. 430 (2021).
[40] M.F. Wang, Z.Y. Hou, A.A. Al Kheraif, B.G. Xing, J. Lin, Mini Review of TiO2-Based Multifunctional Nanocomposites for Near-Infrared Light-Responsive Phototherapy, Adv. Healthc. Mater. 7 (2018).
[41] T.M. Lopez-Goerne, F.J. Padilla-Godinez, M. Castellanos, L.A. Perez-Davalos, Catalytic nanomedicine: a brief review of bionanocatalysts, Nanomedicine (2022).
[42] N. Mas, J.L. Hueso, G. Martinez, A. Madrid, R. Mallada, M.C. Ortega-Liebana, C. Bueno-Alejo, J. Santamaria, Laser-driven direct synthesis of carbon nanodots and application as sensitizers for visible-light photocatalysis, Carbon 156 (2020) 453–462.
[43] M.C. Ortega-Liebana, J.L. Hueso, S. Ferdousi, R. Arenal, S. Irusta, K.L. Yeung, J. Santamaria, Extraordinary sensitizing effect of co-doped carbon nanodots derived from mate herb: application to enhanced photocatalytic degradation of chlorinated wastewater compounds under visible light, Appl. Catal. B-Environ. 218 (2017) 68–79.
[44] M.C. Ortega-Liebana, J.L. Hueso, S. Ferdousi, K.L. Yeung, J. Santamaria, Nitrogen-doped luminescent carbon nanodots for optimal photo-generation of hydroxyl radicals and visible-light expanded photo-catalysis, Diam. Relat. Mater. 65 (2016) 176–182.
[45] M. Carmen Ortega-Liebana, M. Mar Encabo-Berzosa, A. Casanova, M. Desiree Pereboom, J. Octavio Alda, J.L. Hueso, J. Santamaria, Upconverting Carbon Nanodots from Ethylenediaminetetraacetic Acid (EDTA) as Near-Infrared Activated Phototheranostic Agents, Chem. -a Eur. J. 25 (2019) 5539–5546.
[46] H.T. Li, R.H. Liu, S.Y. Lian, Y. Liu, H. Huang, Z.H. Kang, Near-infrared light controlled photocatalytic activity of carbon quantum dots for highly selective oxidation reaction, Nanoscale 5 (2013) 3289–3297.
[47] X. Wu, F. Yu, Y. Han, L. Jiang, Z. Li, J. Zhu, Q. Xu, A.C. Tedesco, J. Zhang, H. Bi, Enhanced chemodynamic and photoluminescence efficiencies of Fe–O4 coordinated carbon dots via the core–shell synergistic effect, Nanoscale 15 (2023) 376–386.
[48] M.C. Ortega-Liebana, M.M. Encabo-Berzosa, M.J. Ruedas-Rama, J.L. Hueso, Nitrogen-induced transformation of vitamin C into multifunctional up-converting carbon nanodots in the visible-NIR range, Chem. -A Eur. J. 23 (2017) 3067–3073.
[49] S.Y. Lim, W. Shen, Z.Q. Gao, Carbon quantum dots and their applications, Chem. Soc. Rev. 44 (2015) 362–381.
[50] G. Wu, T. Nishikawa, B. Ohtani, A. Chen, Synthesis and characterization of carbon-doped TiO2 nanostructures with enhanced visible light response, Chem. Mater. 19 (2007) 4530–4537.
[51] L.H. Shi, Y.Y. Li, X.F. Li, X.P. Wen, G.M. Zhang, J. Yang, C. Dong, S.M. Shuang, Facile and eco-friendly synthesis of green fluorescent carbon nanodots for applications in bioimaging, patterning and staining, Nanoscale 7 (2015) 7394–7401.
[52] H. Maskrot, Y. Leconte, N. Herlin-Boime, C. Reynaud, E. Guelou, L. Pinard, S. Valange, J. Barrault, M. Gervais, Synthesis of nanostructured catalysts by laser pyrolysis, Catal. Today 116 (2006) 6–11.
[53] G. Martinez, A. Malumbres, A. Lopez, R. Mallada, J.L. Hueso, J. Santamaria, Laser-Assisted Production of Carbon-Encapsulated Pt-Co Alloy Nanoparticles for Preferential Oxidation of Carbon Monoxide, Front. Chem. 6 (2018).
[54] A. Malumbres, G. Martinez, J.L. Hueso, J. Gracia, R. Mallada, A. Ibarra, J. Santamaria, Facile production of stable silicon nanoparticles: laser chemistry coupled to in situ stabilization via room temperature hydrosilylation, Nanoscale 7 (2015) 8566–8573.
[55] X. Zhang, S. Wang, G. Cheng, P. Yu, J. Chang, Light-Responsive Nanomaterials for Cancer Therapy, Engineering 13 (2022) 18–30.
[56] L. Da Via, C. Recchi, E.O. Gonzalez-Yanez, T.E. Davies, J.A. Lopez-Sanchez, Visible light selective photocatalytic conversion of glucose by TiO2, Appl. Catal. B-Environ. 202 (2017) 281–288.
[57] B.C.M. Martindale, E. Joliat, C. Bachmann, R. Alberto, E. Reisner, Clean Donor Oxidation Enhances the H-2 Evolution Activity of a Carbon Quantum Dot-Molecular Catalyst Photosystem, Angew. Chem. -Int. Ed. 55 (2016) 9402–9406.
[58] B.C.M. Martindale, G.A.M. Hutton, C.A. Caputo, E. Reisner, Solar hydrogen production using carbon quantum dots and a molecular nickel catalyst, J. Am. Chem. Soc. 137 (2015) 6018–6025.
[59] B.B. Jin, G.D. Yao, X.G. Wang, K.F. Ding, F.M. Jin, Photocatalytic oxidation of glucose into formate on nano TiO2 catalyst, Acs Sustain. Chem. Eng. 5 (2017) 6377–6381.
[60] M.C. Ortega-Liebana, J.L. Hueso, A. Larrea, V. Sebastiana, J. Santamaria, Feroxyhyte nanoflakes coupled to up-converting carbon nanodots: a highly active, magnetically recoverable, Fenton-like photocatalyst in the visible-NIR range, Chem. Commun. 51 (2015) 16625–16628.

[61] M. Scarisoreanu, I. Morjan, R. Alexandrescu, C.T. Fleaca, A. Badoi, E. Dutu, A. M. Niculescu, C. Luculescu, E. Vasile, J. Wang, S. Bouhadoun, N. Herlin-Boime, Enhancing the visible light absorption of titania nanoparticles by S and C doping in a single-step process, Appl. Surf. Sci. 302 (2014) 11–18.
[62] J. Mou, T.Q. Lin, F.Q. Huang, H.R. Chen, J.L. Shi, Black titania-based theranostic nanoplatform for single NIR laser induced dual-modal imaging-guided PTT/PDT, Biomaterials 84 (2016) 13–24.
[63] J. Yin, Q.Q. Zhang, C.J. Yang, B.G. Zhang, K.J. Deng, Highly selective oxidation of glucose to gluconic acid and glucaric acid in water catalyzed by an efficient synergistic photocatalytic system, Catal. Sci. Technol. 10 (2020) 2231–2241.
[64] J.C. Ge, M.H. Lan, B.J. Zhou, W.M. Liu, L. Guo, H. Wang, Q.Y. Jia, G.L. Niu, X. Huang, H.Y. Zhou, X.M. Meng, P.F. Wang, C.S. Lee, W.J. Zhang, X.D. Han, A graphene quantum dot photodynamic therapy agent with high singlet oxygen generation, Nat. Commun. 5 (2014).
[65] J. Bonet-Aleta, J.I. Garcia-Peiro, J.L. Hueso, Engineered Nanostructured Photocatalysts for Cancer Therapy, Catalysts 12 (2022).
[66] A. Cios, M. Ciepielak, A. Szymański, S. Lewicka, W. Cierniak, M. Stankiewicz, S. Mendrycka, Lewicki, Effect of Different Wavelengths of Laser Irradiation on the Skin Cells, Int. J. Mol. Sci. (2021).
[67] Y. Ding, J. Yu, X. Chen, S. Wang, Z. Tu, G. Shen, H. Wang, R. Jia, S. Ge, J. Ruan, K. W. Leong, X. Fan, Dose-Dependent Carbon-Dot-Induced ROS Promote Uveal Melanoma Cell Tumorigenicity via Activation of mTOR Signaling and Glutamine Metabolism, Adv. Sci. 8 (2021) 2002404.
[68] X.Z. Yuan, J. Zhang, M. Yan, M.Y. Si, L.B. Jiang, Y.F. Li, H.B. Yu, J. Zhang, G. M. Zeng, Nitrogen doped carbon quantum dots promoted the construction of Z-scheme system with enhanced molecular oxygen activation ability, J. Colloid Interface Sci. 541 (2019) 123–132.
[69] C. Disdier, J. Devoy, A. Cosnefroy, M. Chalansonnet, N. Herlin-Boime, E. Brun, A. Lund, A. Mabondzo, Tissue biodistribution of intravenously administrated titanium dioxide nanoparticles revealed blood-brain barrier clearance and brain inflammation in rat, Part. Fibre Toxicol. 12 (2015).
[70] M. Dorier, D. Beal, C. Tisseyre, C. Marie-Desvergne, M. Dubosson, F. Barreau, E. Houdeau, N. Herlin-Boime, T. Rabilloud, M. Carriere, The food additive E171 and titanium dioxide nanoparticles indirectly alter the homeostasis of human intestinal epithelial cells in vitro, Environ. Sci. -Nano 6 (2019) 1549–1561.
[71] M.L. Jugan, S. Barillet, A. Simon-Deckers, N. Herlin-Boime, S. Sauvaigo, T. Douki, M. Carriere, Titanium dioxide nanoparticles exhibit genotoxicity and impair DNA repair activity in A549 cells, Nanotoxicology 6 (2012) 501–513.
[72] T. Lopez-Goerne, P. Ramirez, D. Alvarez, F. Rodriguez-Reinoso, A.M. Silvestre-Albero, E. Gomez, E. Rodriguez-Castellon, Physicochemical properties and in vivo evaluation of Pt/TiO2-SiO2 nanopowders, Nanomedicine 13 (2018) 2171–2186.
[73] A. Martín-Pardillos, A. Tsaalbi-Shtylik, S. Chen, et al., Genomic and functional integrity of the hematopoietic system requires tolerance of oxidative DNA lesions, Blood. 2017;130(13):1523-1534, Blood 131 (2018), 710-710.
[74] U.S. Srinivas, B.W.Q. Tan, B.A. Vellayappan, A.D. Jeyasekharan, ROS and the DNA damage response in cancer, Redox Biol. 25 (2019), 101084.
[75] M. Podhorecka, A. Skladanowski, P. Bozko, H2AX phosphorylation: its role in DNA damage response and cancer therapy, J. Nucleic Acids 2010 (2010), 920161.
[76] C.E. Redon, J.S. Dickey, W.M. Bonner, O.A. Sedelnikova, γ-H2AX as a biomarker of DNA damage induced by ionizing radiation in human peripheral blood lymphocytes and artificial skin, Adv. Space Res. 43 (2009) 1171–1178.
[77] L.G. Mariotti, G. Pirovano, K.I. Savage, M. Ghita, A. Ottolenghi, K.M. Prise, G. Schettino, Use of the γ-H2AX Assay to Investigate DNA Repair Dynamics Following Multiple Radiation Exposures, PLOS ONE 8 (2013), e79541.
[78] C.A. Juan, J.M. Pérez de la Lastra, F.J. Plou, E. Pérez-Lebeña, The chemistry of reactive oxygen species (ROS) revisited: outlining their role in biological macromolecules (DNA, Lipids and Proteins) and induced pathologies, Int. J. Mol. Sci. (2021).
[79] A.S. Bader, B.R. Hawley, A. Wilczynska, M. Bushell, The roles of RNA in DNA double-strand break repair, Br. J. Cancer 122 (2020) 613–623.
[80] O. Surova, B. Zhivotovsky, Various modes of cell death induced by DNA damage, Oncogene 32 (2013) 3789–3797.
[81] T.C. Long, N. Saleh, R.D. Tilton, G.V. Lowry, B. Veronesi, Titanium dioxide (P25) produces reactive oxygen species in immortalized brain microglia (BV2): implications for nanoparticle neurotoxicity, Environ. Sci. Technol. 40 (2006) 4346–4352.